Hindawi
Journal of Nanomaterials
Volume 2019, Article ID 4702849, 8 pages
https://doi.org/10.1155/2019/4702849

Research Article

Synthesis of ZnO/Polypyrrole Nanoring Composite as High-Performance Anode Materials for Lithium Ion Batteries

Haipeng Li,[1] Shuang Yang,[1] Yan Zhao,[1] Taizhe Tan,[2] Xin Wang,[3] and Zhumabay Bakenov[4]

[1]*School of Materials Science and Engineering, Hebei University of Technology, Tianjin 300130, China*
[2]*Synergy Innovation Institute of GDUT, Heyuan, 517000 Guangdong Province, China*
[3]*International Academy of Optoelectronics at Zhaoqing, South China Normal University, Guangdong Province, China*
[4]*School of Engineering, Nazarbayev University, Institute of Batteries LLC, National Laboratory Astana, 53 Kabanbay Batyr Avenue, Astana 010000, Kazakhstan*

Correspondence should be addressed to Yan Zhao; yanzhao1984@hebut.edu.cn and Xin Wang; wangxin@scnu.edu.cn

Received 16 July 2018; Accepted 25 November 2018; Published 3 March 2019

Academic Editor: Ovidiu Ersen

ZnO has attracted considerable attention as electrode material in lithium-ion battery (LIB) due to its theoretically high capacity. However, poor electronic conductivity and huge volumetric changes during cycling limit its industrial applications. In this work, polypyrrole nanorings (PNRs) were successfully prepared via the solution chemistry method using pyrrole (Py) as raw material, ammonium persulfate (APS) as oxidant, and cetyltrimethyl ammonium bromide (CTAB) as surfactant. The ZnO/PNR composite was synthesized with zinc oxide nanoparticles absorbed on the surface of PPy nanorings through the one-pot in situ sol-gel method. The composite shows a three-dimensional intertwined network structure where the size of polypyrrole nanorings ranges from 80 nm to 100 nm in diameter and the average size of uniformly distributed ZnO nanocrystals is 10.49 nm. The unique three-dimensional conductive framework can provide good electronic contact between the ZnO particles and buffer the volume variation during the lithiation/delithiation processes. As an electrode material for LIBs, the ZnO/PNR composite delivers a first cycle discharge capacity of 1658 mAh g^{-1} and a capacity retention of 50.7% over 150 cycles at 200 mA g^{-1}, indicating high specific capacity and outstanding cycle stability.

1. Introduction

The current interest in electric vehicles and portable electronics has prompted the demand for lithium-ion batteries (LIBs) with large energy/power density as well as long lifetime [1–3]. Recently, transition metal oxides such as SnO_2 [4], Fe_2O_3 [5], MnO_2 [6], and ZnO [7] have been explored as promising alternative anodes because of their high theoretical capacities, which are several times higher than those of the conventional carbon (372 mAh g^{-1}). Among these numerous anode candidates, ZnO has been widely studied due to its relatively high theoretical capacity (978 mAh g^{-1}), abundant sources, cost-effectiveness, and chemical stability [8–10]. However, pure ZnO electrodes exhibit a rapid capacity decay and inferior rate capability because of low electrical conductivity and huge volumetric expansion/contraction during the charge/discharge processes [11–14].

To alleviate these issues, the strategy of decreasing particle size of ZnO to nanometer range is a well-accepted approach to not only provide a short diffusion path for Li^+ but also accommodate the volume expansion during lithiation/delithiation [15–17]. Furthermore, encapsulating ZnO into various conductive and elastic materials can also provide a robust network to enhance the electrical conductivity and prevent the ZnO particles from agglomeration [18–20]. Among these network materials, conducting polymers have been considered as a potential additive to improve the anode performance in LIBs because of their good conductivity (10-100 S cm^{-1}) and high chemical stability [21, 22]. PPy has been successfully introduced to

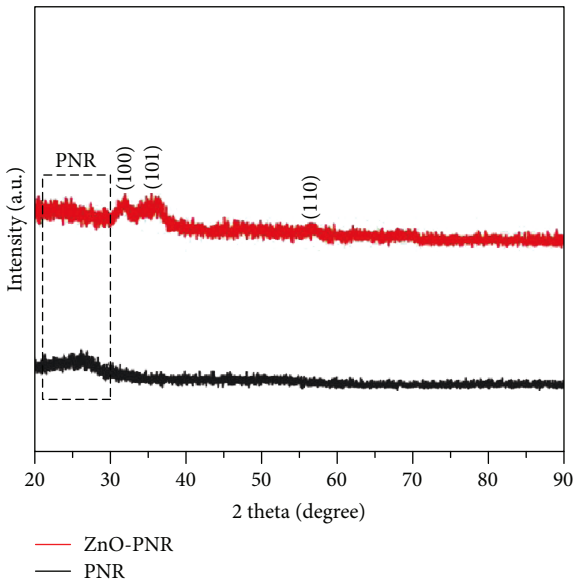

Figure 1: XRD characterization of pure PNR and ZnO/PNR.

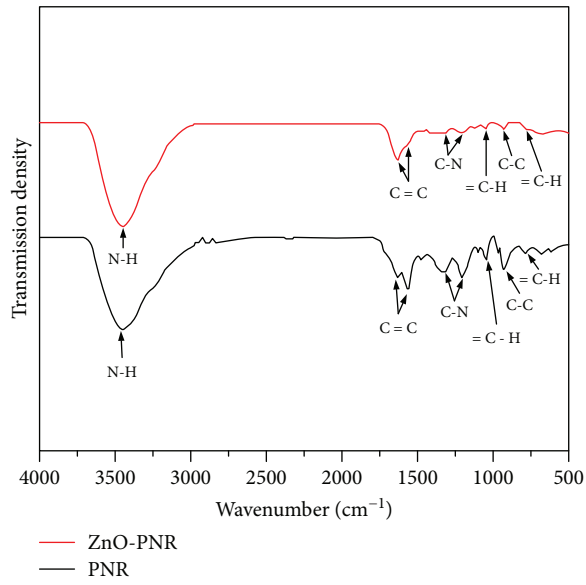

Figure 2: FT-IR spectra of pure PNR and ZnO/PNR composite.

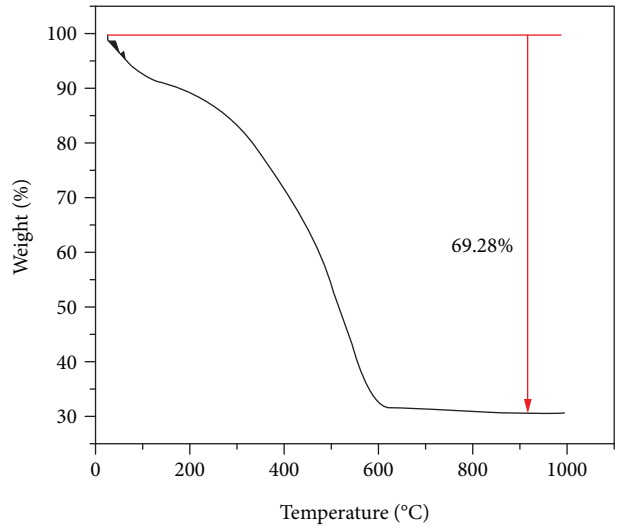

Figure 3: TGA curve of ZnO/PNR composite.

enhance the anode performance in LIBs; for instance, SnO_2/PPy [23], MnO_2/PPy [24], and NiO/PPy [25] have exhibited both significant electrical conductivity and electrochemical activity.

Herein, we have proposed a simple and reproducible method to prepare PPy nanorings (PNRs) as a support for ZnO nanoparticles. PNRs form a three-dimensional intertwined network structure with numerous nanorings. The ZnO nanoparticles for homogenous distribution on the PNR matrix were obtained via one-pot sol-gel synthesis route. The resultant ZnO/PNR composite exhibits three-dimensional macroporous structure of PNR with uniformly distributed ZnO nanoparticles on its surface. ZnO nanoparticles combined with three-dimensional network structure of PNR demonstrate superior cycling stability, excellent Li storage performance, and high rate capability when applied to anode materials of LIBs. The observations can be attributed to the structure—determining larger electrode/electrolyte interface, higher conductivity, stronger mechanical strength, and shorter ion transport pathway.

2. Experimental

2.1. PNR Preparation. In a typical procedure, 0.2853 g (0.783 mmol) of CTAB was mixed with 100 mL of distilled water to obtain a 7.83 mM CTAB solution. Then, 333 mL of 30 mM Py monomer solution was mixed with the CTAB solution, and the resultant solution was vigorously stirred at temperature of 0-5°C for 3 h. After that, 50 mL of 0.1 mM APS solution was added dropwise into the resultant mixture and stirred at the same temperature for another 24 h. Finally, the resultant material was rinsed thoroughly with deionized water and dried at 60°C to obtain the PNR products.

2.2. Synthesis of ZnO/PNR Composite. For the preparation of the ZnO/PNR composite, 0.1932 g (0.88 mmol) of Zn $(CH_3COO)_2{\cdot}2H_2O$ was added into 50 mL methyl alcohol, 0.1192 g (2.1 mmol) KOH was added into 40 mL methyl alcohol, and both the mixtures were stirred vigorously at 60°C to form homogeneous $Zn(CH_3COO)_2$ solution (17.6 mM) and KOH solution (52.5 mM). Then, 0.2 g PNR was dispersed in another 30 mL methyl alcohol via ultrasonication for 0.5 h and mixed with the prepared $Zn(CH_3COO)_2$ solution. Afterwards, the mixture was stirred for 0.5 h at 60°C, followed by slow addition of the KOH solution under gentle agitation. The total mixture was then stirred continuously for 2 h at 60°C. Finally, the precipitate was centrifuged, rinsed with ultrapure water, and dried at 60°C overnight.

2.3. Structure Characterization. The crystalline phase of the as-prepared samples was probed with a XRD diffractometer (Bruker D8) with Cu Kα radiation. Infrared absorption spectra were recorded on a FTIR spectrometer (FTIR, Nicolet iS10, USA) at room temperature. The ZnO content in the

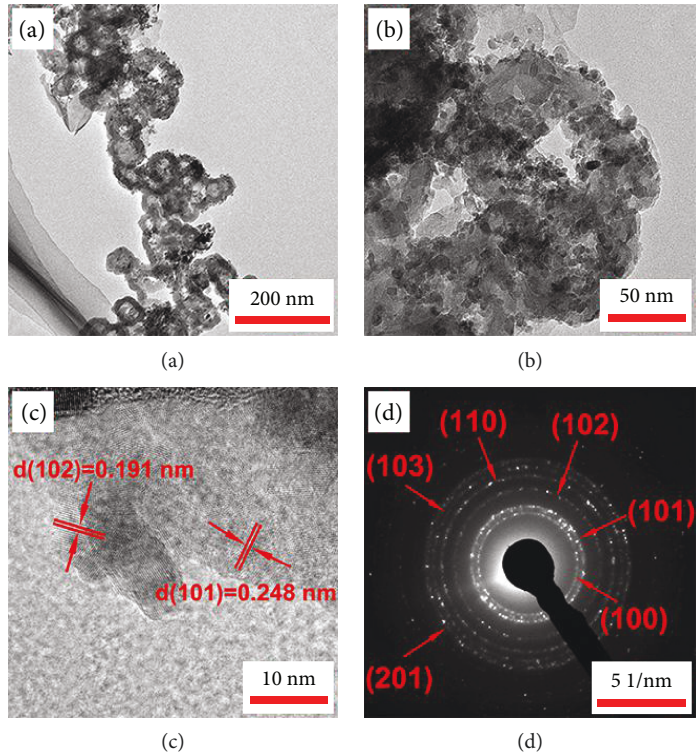

Figure 4: (a, b) TEM images at different magnifications, (c) high-resolution TEM (HRTEM) image, and (d) selected area electron diffraction (SAED) pattern of ZnO/PNR.

composite was measured with a thermogravimetric analyzer (TGA) (STA 409 PC Luxx, Germany) in air (heating rate: 10°C min^{-1}). The morphology and physical microstructure of the sample were observed by transmission electron microscopy (TEM, JEM-2100F, JEOL). X-ray photoelectron spectrometer (XPS) was conducted to evaluate the surface compositions of the samples. The surface area and pore size distribution were recorded by the Brunauer-Emmett-Teller (BET) method and the Barrett-Joyner-Halenda (BJH) method, respectively.

2.4. Electrochemical Measurements. For the preparation of the electrode, the as-synthesized materials, acetylene black, and polyvinylidene fluoride binder were added into a blend solution using N-methyl-2-pyrrolidone (NMP) as a solvent to form a homogeneous slurry at weight percent of 8 : 1 : 1. This thoroughly mixed slurry was coated on an aluminum foil. After drying at 60°C overnight under vacuum, the electrode was cut into circular strips of 8 mm diameter and used as the working electrode. The mass loading of active material in each electrode was about 1.7 mg cm^{-2}. Lithium sheets were used for the combined counter and reference electrodes while the separator was a microporous polyethylene film (Celgard 2300). The solution of 1 M $LiPF_6$ in mixed ethylene carbonate (EC) and dimethyl carbonate (DMC) (1 : 1 *v*/*v*) was used as an electrolyte. To investigate the electrochemical performances, CR2032 coin-type cells were sealed in an argon-filled glovebox and tested galvanostatically on a Neware BTS test system (Shenzhen, China) with a voltage window of 0.01 V-3.0 V.

3. Results and Discussion

The XRD patterns revealed the crystalline structures of pure PNR and ZnO/PNR composite. As shown in Figure 1, pure PNR has no other diffraction peaks except for a broad and weak diffraction peak centered at 26°, which is attributed to the p-p interaction of partial PPy chains, indicating an amorphous structure [26, 27]. In the case of ZnO/PNR composite, the peaks centered at $2\theta = 31.8°$, 36.3°, and 56.6° agree well with the crystal planes of (100), (101), and (110) in hexagonal wurtzite ZnO (JCPDS no. 36-1451) [12]. Moreover, the diminished intensity of PNR diffraction peak in ZnO/PNR nanocomposites can be attributed to the existence of ZnO nanoparticles and partial concealing of PNR by ZnO nanoparticles. The diffraction intensity of ZnO in ZnO/PNR composite showed weak and broad XRD peaks, which may be connected with homogeneous distribution and small particle size of ZnO [28]. No peaks corresponding to any impurity were found, implying the high purity of the product.

To further determine the chemical structure of PNR, both the PNR and ZnO/PNR composite were investigated with FTIR spectroscopy in the wavelength range of 4000-500 cm^{-1}. As shown in Figure 2, the band at around 3442 cm^{-1} can be assigned to the N-H stretching mode, which is the characteristic peak of PNR. The peaks centered at 1636 cm^{-1} and 1564 cm^{-1} correspond to the stretching vibration of C=C bond in the pyrrole rings. The C-N stretching vibrations can be observed at 1325 cm^{-1} and 1207 cm^{-1}. The peaks at 1047 cm^{-1} and 792 cm^{-1} are associated with the vibration of =C-H, and the peak located at 927 cm^{-1}

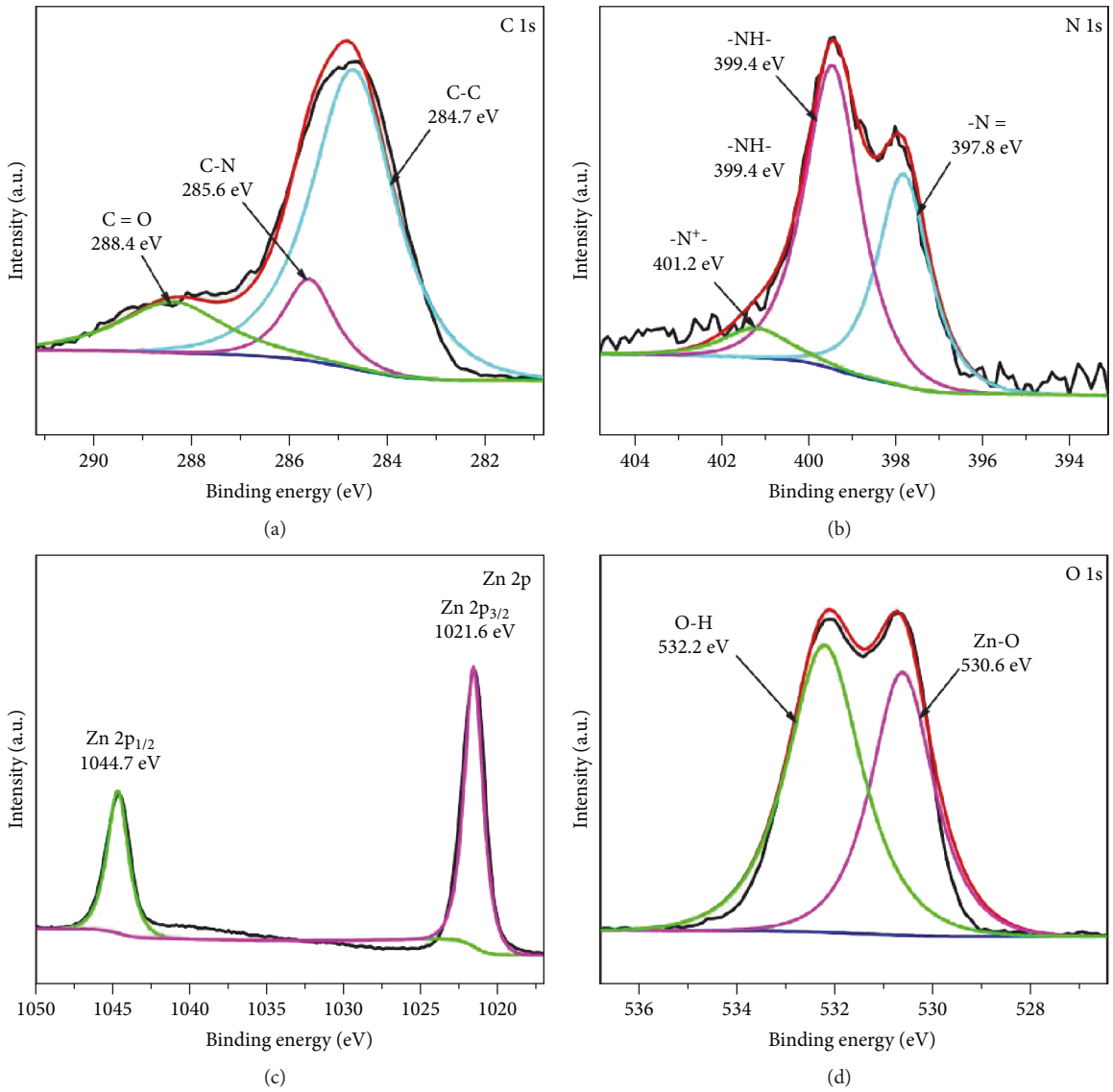

Figure 5: (a) C 1s, (b) N 1s, (c) Zn 2p, and (d) O 1s spectra of ZnO/PNR composite.

originates from the C-C out of phase [29–34]. Consequently, we can conclude that we have successfully synthesized PNR by experimentation. The intensity of these characteristic bands is lower than pure PNR, which may be due to a lower PNR content in the ZnO/PNR composite. Furthermore, FTIR spectra of ZnO/PNR composite exhibited a little blue shift because of the introduction of ZnO. The vibration of =C-H is shifted from 1047 cm^{-1} and 792 cm^{-1} to 1044 cm^{-1} and 773 cm^{-1}. The C-N stretching vibrations are shifted from 1325 cm^{-1} and 1207 cm^{-1} to 1317 cm^{-1} and 1205 cm^{-1}. All the blue shifts indicate a strong interaction between PNR and ZnO [29–31].

The obtained TGA curve is shown in Figure 3. The as-prepared sample was heated from 25°C to 1000°C under air atmosphere. The ZnO/PNR composite displayed two weight loss regions. The initial weight loss occurred between 25 and 120°C due to the evaporation of absorbed water. The second weight loss region began at 120°C and ended at 610°C, which can be assigned to thermal decomposition of PNR chains. The weight percentage of ZnO in the composite as per the TGA analysis is about 30.72 wt%.

TEM and HRTEM were employed to discern the morphologies of ZnO/PNR. As presented in Figure 4(a), the polypyrrole nanorings intertwine to form a uniform macroporous network with the size of around 100 nm. Moreover, it can be seen that the ultrasmall crystalline particles dispersed homogeneously on the surface of the polypyrrole nanorings without serious agglomeration. The polypyrrole matrix is important because it forms ZnO nanocrystal interconnection with the three-dimensional (3D) interconnected porous structure. Thus, this unique structure is beneficial to provide fast ionic transfer channels and retain internal void spaces to accommodate the severe volume change, leading to enhancement of reversible capacity and cycling performance. The nanoparticles have a diameter range of 8~16 nm (see TEM image of Figure 4(b)). As shown in Figure 4(c), the HRTEM image exhibits the measured d -spacing of 0.191 nm and 0.248 nm, which correspond to

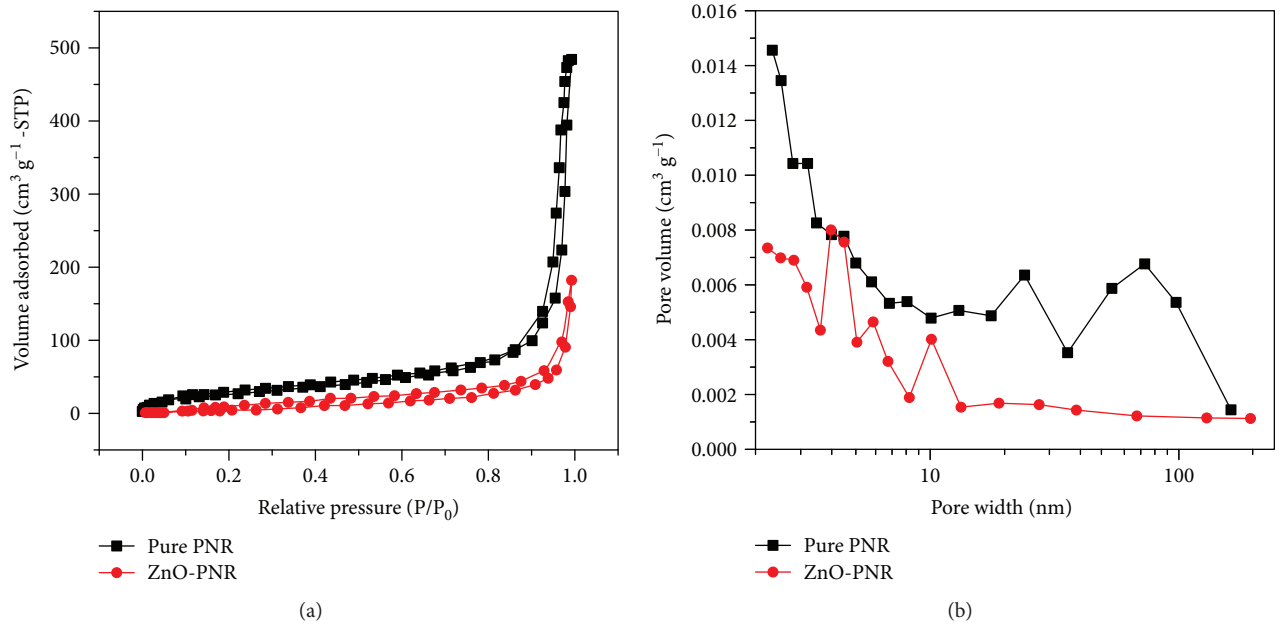

Figure 6: Nitrogen adsorption/desorption isotherms (a) and pore size distribution (b) of pure PNR and ZnO/PNR.

the (102) and (101) planes of ZnO, respectively, suggesting the successful formation of ZnO nanoparticles [14]. The selected area electron diffraction pattern (Figure 4(d)) was used to further confirm the formation of single crystal ZnO nanocrystal as the diffraction rings in the SAED pattern can be indexed as ZnO phase.

The XPS analysis was carried out to investigate the chemical state of ZnO/PNR composite. C 1s, N 1s, Zn 2p, and O 1s signals were detected. The C 1s spectrum presented two resolved binding energies centered at 284.7 and 288.4 eV, which are ascribed to C-C and C=O, respectively. Besides, the characteristic peak of C-N bonding located at 285.6 eV corroborates the existence of PNR in the ZnO/PNR material [35]. Similarly, the XPS spectrum of N 1s can be further separated into three components. Three peaks are located at 397.8, 399.5, and 401.2 eV, respectively, which are in accordance with the -N=, -NH-, and -N^+- [36]. The fitting peaks located at 1021.6 and 1044.7 eV in Figure 5(c) are assigned to the spin orbit peaks of Zn 2p3/2 and Zn 2p1/2 in ZnO, respectively, indicating the typical ZnO phase. While the peak at 530.6 eV in Figure 5(d) is related to Zn-O, suggesting that ZnO nanoparticles are formed. The peak at 532.2 eV is usually identified as the O-H bond of surface-adsorbed water [37]. The XPS results were aligned with the above presented XRD and FTIR data.

The nitrogen adsorption-desorption isotherms were obtained to investigate the porosity and surface structure of pure PNR and ZnO/PNR composite. As shown in Figure 6(a), the BET specific surface area of the as-obtained products decreased from 103.17 to 28.00 m^2 g^{-1} due to the formation of ZnO nanoparticles within the porous channels of PNR, which is consistent with the conclusion of TEM results. The pore size distributions in Figure 6(b) were calculated from the desorption data using the BJH method. The primary pore size distribution of pure PNR ranges from 2.3 nm to 73.8 nm, while ZnO/PNR presented mesoporous characteristics (2.3-24.3 nm). A portion of mesopores and nearly all the macropores disappeared as compared with pure PNR, which can be attributed to the impregnation of ZnO nanoparticles into the pores and surface of PNR. The mesoporous structure of ZnO/PNR composite can provide efficient transport of ions into the electrode material leading to a high electrochemical capacitance. Moreover, the reserved internal space is conducive to alleviate the large volume variation during the charge-discharge process [38, 39].

The charge-discharge behavior of the ZnO/PNR composite was examined between 0.01 V and 3 V at 200 mA g^{-1}. The 1st, 2nd, and 3rd cycle galvanostatic cycling profiles of the investigated anode are shown in Figure 7(a). In the first discharge cycle, a clear slope starting at around 0.8 V is due to the reduction of ZnO to Zn ($ZnO + 2Li \longrightarrow Zn + Li_2O$) and the LiZn alloying reaction ($Zn + xLi \longrightarrow Li_xZn$), while a wide discharge voltage plateau at 0.5 V can be attributed to the solid electrolyte interphase (SEI) film formation [15, 40]. In the following cycles, the plateau located at 0.5 V disappeared, which reflects the initial irreversible capacity loss caused by the formation of SEI film [41]. In the charge process, there is an unconspicuous slope starting at around 0.23 V, which corresponds to the multistep dealloying reactions of LiZn alloy, like $LiZn \longrightarrow Li_2Zn_3 \longrightarrow LiZn_2 \longrightarrow Li_2Zn_5 \longrightarrow Zn$ [14]. Besides, the voltage plateau appeared at 1.2 V can be assigned to the formation of ZnO [42]. In conclusion, the Li storage mechanism of ZnO can be expressed as follows:

$$\begin{aligned} ZnO + 2Li &\leftrightarrow Zn + Li_2O \\ Zn + Li &\leftrightarrow LiZn \end{aligned} \quad (1)$$

Also, the ZnO/PNR composite exhibited the first discharge capacity of 1658 mAh g^{-1}, which is above the

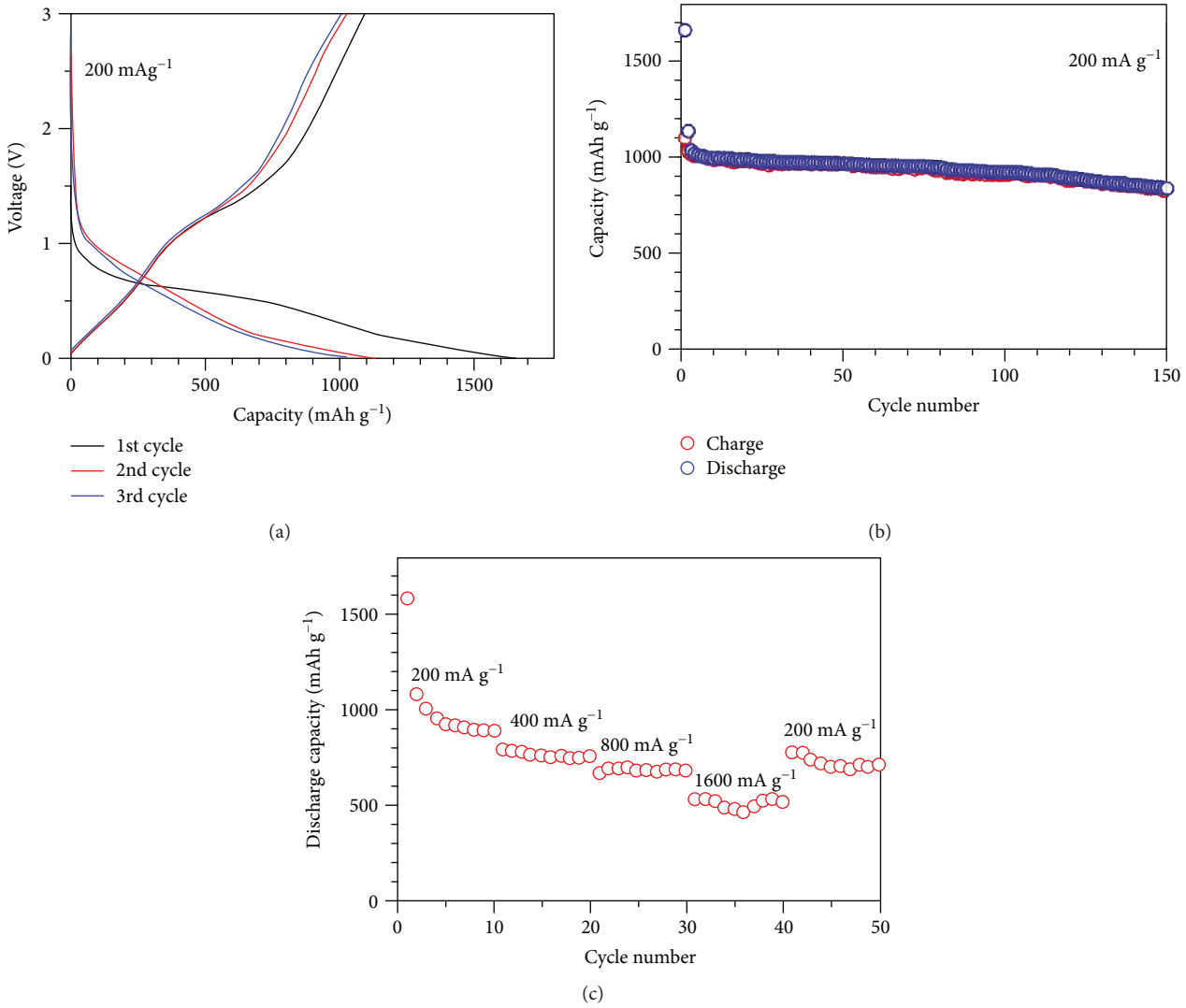

Figure 7: Electrochemical performance of ZnO/PNR electrode: (a) the initial three discharge and charge curves, (b) cycle performance at 200 mA g^{-1} between 0.01 V and 3.0 V, and (c) discharge rate performance at different current densities.

theoretical value for ZnO (978 mAh g^{-1}). The charge capacity in the first cycle is 1095 mAh g^{-1}, which corresponds to an initial coulombic efficiency of 66%. The irreversible capacity losses can be due to the generation of SEI film owing to the electrolyte decomposition and the irreversible process of Li_2O formation, which is common for transition metal oxides [14]. However, in the subsequent discharge-charge cycles, the discharge curves are different from the first one but become almost identical in terms of size and shape, indicating a good reversibility of the redox processes of ZnO/PNR composite [13]. Figure 7(b) illustrates the cycle performance of the ZnO/PNR electrode at 200 mA g^{-1}. ZnO/PNR suffers a rapid capacity decline in the initial 5 cycles, which may be because of the irreversible reactions and morphological changes during the charge-discharge processes. Subsequently, the capacity decays slowly and stabilizes at 840 mAh g^{-1} after 150 cycles, which is over twice as high as that of the commercial graphite (372 mAh g^{-1}), corresponding to the capacity retention of 50.7% relative to the initial charge capacity. The excellent cycle behavior of the ZnO/PNR electrode can be ascribed to the nanosize of ZnO particles synthesized in this work, which has more contact area with the surface of PNR and shortens the diffusion paths for Li^+ when tested as anodes in LIBs. Furthermore, both the large specific surface area and porous nanostructure can prevent the aggregation of ZnO nanoparticles and accommodate the volume expansion/shrinkage during the continuous charge/discharge processes, and as a result, mitigate the sharp capacity fading.

The rate capability of the synthesized ZnO/PNR composite is exhibited in Figure 7(c). As the current density increases from 200, 400, 800 to 1600 mA g^{-1}, the average capacity of 952, 777, 693, and 528 mAh g^{-1} are obtained, respectively, which are much higher than those previously reported [43–45]. The capacity of 718 mAh g^{-1} can be recovered when the current density is turned back to 200 mA g^{-1}, demonstrating an excellent electrochemical reversibility and well structural integrity of the anode material.

4. Conclusion

In conclusion, we demonstrated the fabrication of polypyrrole with three-dimensional intertwined network using the solution chemistry method. The composite of microsized hexagonal ZnO nanoparticles absorbed on the surface of polypyrrole nanorings was prepared by an in situ sol-gel method. When employed as an electrode material in LIBs, ZnO/PNR composite illustrated superior reversible capacities and impressive cycling performance. After 150 cycles, a relatively high discharge capacity of 840 mAh g^{-1} could be harvested at 200 mA g^{-1}. Such a good cyclic performance could be due to the interconnected 3D architecture of polypyrrole nanorings and synergistic interaction between ZnO and PNR to obtain highly dispersed ZnO nanoparticles, enhance the electrical conductivity of ZnO, and accommodate the volume variation during the charge-discharge processes. Thus, LIBs based on the ZnO/PNR composite can have promising applications.

Data Availability

The data used to support the findings of this study are included within the article.

Conflicts of Interest

The authors declare that there is no conflict of interests regarding the publication of this paper.

Acknowledgments

The authors acknowledge the financial support from the Program for the Outstanding Young Talents of Hebei Province, Hebei Province Natural Science Foundation of China (Project no. E2015202037), Science and Technology Correspondent Project of Tianjin (Project no. 14JCTPJC00496), Cultivation Project of National Engineering Technology Center (2017B090903008), and the targeted funding program "Innovative Materials and Systems for Energy Conversion and Storage" by the Ministry of Education and Science of the Republic of Kazakhstan.

References

[1] J. Cabana, L. Monconduit, D. Larcher, and M. R. Palacín, "Beyond intercalation-based Li-ion batteries: the state of the art and challenges of electrode materials reacting through conversion reactions," *Advanced Materials*, vol. 22, no. 35, pp. E170–E192, 2010.

[2] J. B. Goodenough and K. S. Park, "The Li-ion rechargeable battery: a perspective," *Journal of the American Chemical Society*, vol. 135, no. 4, pp. 1167–1176, 2013.

[3] Y. Tian, Z. Sun, Y. Zhang, X. Wang, Z. Bakenov, and F. Yin, "Micro-spherical sulfur/graphene oxide composite via spray drying for high performance lithium sulfur batteries," *Nanomaterials*, vol. 8, no. 1, p. 50, 2018.

[4] M. S. Park, G. X. Wang, Y. M. Kang, D. Wexler, S. H. Dou, and H. K. Liu, "Preparation and electrochemical properties of SnO_2 nanowires for application in lithium-ion batteries," *Angewandte Chemie International Edition*, vol. 46, no. 5, pp. 750–753, 2007.

[5] M. V. Reddy, T. Yu, C. H. Sow et al., "α-Fe_2O_3 nanoflakes as an anode material for Li-ion batteries," *Advanced Functional Materials*, vol. 17, no. 15, pp. 2792–2799, 2010.

[6] S. Suzuki, S. Takahashi, K. Sato, and M. Miyayama, "High-rate electrode properties of Li-Mn-oxide synthesized by reassembly of MnO_2 nanosheets for Li-ion battery," *Key Engineering Materials*, vol. 320, pp. 223–226, 2006.

[7] M. Ahmad, Y. Shi, A. Nisar, and H. Sun, "Synthesis of hierarchical flower-like ZnO nanostructures and their functionalization by au nanoparticles for improved photocatalytic and high performance Li-ion battery anodes," *Journal of Materials Chemistry*, vol. 21, no. 21, pp. 7723–7729, 2011.

[8] H. Wang, Q. Pan, Y. Cheng, J. Zhao, and G. Yin, "Evaluation of ZnO nanorod arrays with dandelion-like morphology as negative electrodes for lithium-ion batteries," *Electrochimica Acta*, vol. 54, no. 10, pp. 2851–2855, 2009.

[9] C. Q. Zhang, J. P. Tu, X. H. Huang, Y. F. Yuan, X. T. Chen, and F. Mao, "Electrochemical performances of Ni-coated ZnO as an anode material for lithium-ion batteries," *Journal of The Electrochemical Society*, vol. 154, no. 2, pp. A65–A69, 2007.

[10] S. M. Abbas, S. Hussain, S. Ali, N. Ahmad, N. Ali, and S. Abbas, "Structure and electrochemical performance of ZnO/CNT composite as anode material for lithium-ion batteries," *Journal of Materials Science*, vol. 48, no. 16, pp. 5429–5436, 2013.

[11] H. Li, Y. Wei, Y. Zhang et al., "In situ, sol-gel synthesis of ultrafine ZnO nanocrystals anchored on graphene as anode material for lithium-ion batteries," *Ceramics International*, vol. 42, no. 10, pp. 12371–12377, 2016.

[12] N. Garino, A. Lamberti, R. Gazia, A. Chiodoni, and C. Gerbaldi, "Cycling behaviour of sponge-like nanostructured ZnO as thin-film Li-ion battery anodes," *Journal of Alloys and Compounds*, vol. 615, pp. S454–S458, 2014.

[13] H. Li, Y. Wei, Y. Zhang et al., "Synthesis and electrochemical investigation of highly dispersed ZnO nanoparticles as anode material for lithium-ion batteries," *Ionics*, vol. 22, no. 8, pp. 1387–1393, 2016.

[14] Y. Zhang, Y. Wei, H. Li, Y. Zhao, F. Yin, and X. Wang, "Simple fabrication of free-standing ZnO/graphene/carbon nanotube composite anode for lithium-ion batteries," *Materials Letters*, vol. 184, pp. 235–238, 2016.

[15] S. Kundu, S. Sain, M. Yoshio, T. Kar, N. Gunawardhana, and S. K. Pradhan, "Structural interpretation of chemically synthesized ZnO nanorod and its application in lithium ion battery," *Applied Surface Science*, vol. 329, pp. 206–211, 2015.

[16] C. T. Hsieh, C. Y. Lin, Y. F. Chen, and J. S. Lin, "Synthesis of ZnO@Graphene composites as anode materials for lithium ion batteries," *Electrochimica Acta*, vol. 111, pp. 359–365, 2013.

[17] M. O. Guler, T. Cetinkaya, U. Tocoglu, and H. Akbulut, "Electrochemical performance of MWCNT reinforced ZnO anodes for Li-ion batteries," *Microelectronic Engineering*, vol. 118, pp. 54–60, 2014.

[18] E. Quartarone, V. Dall'Asta, A. Resmini et al., "Graphite--coated ZnO nanosheets as high-capacity, highly stable, and binder-free anodes for lithium-ion batteries," *Journal of Power Sources*, vol. 320, pp. 314–321, 2016.

[19] Z. Xiu, M. H. Alfaruqi, J. Gim et al., "MOF-derived mesoporous anatase TiO_2 as anode material for lithium–ion batteries with high rate capability and long cycle stability," *Journal of Alloys and Compounds*, vol. 674, pp. 174–178, 2016.

[20] L. Jacob, K. Prasanna, M. R. Vengatesan, P. Santhoshkumar, C. W. Lee, and V. Mittal, "Binary Cu/ZnO decorated graphene nanocomposites as an efficient anode for lithium ion batteries," *Journal of Industrial and Engineering Chemistry*, vol. 59, pp. 108–114, 2017.

[21] M. Rajesh, J. Raj, B. C. Kim, B. B. Cho, J. M. Ko, and K. H. Yu, "Supercapacitive studies on electropolymerized natural organic phosphate doped polypyrrole thin films," *Electrochimica Acta*, vol. 220, pp. 373–383, 2016.

[22] Y. Wei, Q. Hu, Y. Cao et al., "Polypyrrole nanotube arrays on carbonized cotton textile for aqueous sodium battery," *Organic Electronics*, vol. 46, pp. 211–217, 2017.

[23] L. Zhang, K. Zhao, W. Xu et al., "Integrated SnO_2 nanorod array with polypyrrole coverage for high-rate and long-life lithium batteries," *Physical Chemistry Chemical Physics*, vol. 17, no. 12, pp. 7619–7623, 2015.

[24] R. K. Sharma, A. C. Rastogi, and S. B. Desu, "Manganese oxide embedded polypyrrole nanocomposites for electrochemical supercapacitor," *Electrochimica Acta*, vol. 53, no. 26, pp. 7690–7695, 2008.

[25] A. C. Sonavane, A. I. Inamdar, D. S. Dalavi, H. P. Deshmukh, and P. S. Patil, "Simple and rapid synthesis of NiO/PPy thin films with improved electrochromic performance," *Electrochimica Acta*, vol. 55, no. 7, pp. 2344–2351, 2010.

[26] F. Yin, X. Liu, Y. Zhang et al., "Well-dispersed sulfur anchored on interconnected polypyrrole nanofiber network as high performance cathode for lithium-sulfur batteries," *Solid State Sciences*, vol. 66, pp. 44–49, 2017.

[27] W. Yang, W. Yang, J. Feng, and X. Qin, "A polypyrrole-coated acetylene black/sulfur composite cathode material for lithium-sulfur batteries," *Journal of Energy Chemistry*, vol. 27, no. 3, pp. 813–819, 2017.

[28] Q. Li, H. Zhang, S. Lou et al., "Pseudocapacitive Li^+ intercalation in ZnO/ZnO@C composites enables high-rate lithium-ion storage and stable cyclability," *Ceramics International*, vol. 43, no. 15, pp. 11998–12004, 2017.

[29] S. Jain, N. Karmakar, A. Shah, D. C. Kothari, S. Mishra, and N. G. Shimpi, "Ammonia detection of 1-D ZnO/polypyrrole nanocomposite: effect of CSA doping and their structural, chemical, thermal and gas sensing behavior," *Applied Surface Science*, vol. 396, pp. 1317–1325, 2017.

[30] A. Olad and S. Shakoori, "Electromagnetic interference attenuation and shielding effect of quaternary epoxy-PPy/-Fe_3O_4-ZnO nanocomposite as a broad band microwave-absorber," *Journal of Magnetism and Magnetic Materials*, vol. 458, pp. 335–345, 2018.

[31] Z. Wang, P. Xiao, L. Qiao et al., "Polypyrrole sensitized ZnO nanorod arrays for efficient photo-electrochemical splitting of water," *Physica B Condensed Matter*, vol. 419, pp. 51–56, 2013.

[32] M. A. Chougule, S. Sen, and V. B. Patil, "Polypyrrole-ZnO hybrid sensor: effect of camphor sulfonic acid doping on physical and gas sensing properties," *Synthetic Metals*, vol. 162, no. 17-18, pp. 1598–1603, 2012.

[33] A. Pruna, Q. Shao, M. Kamruzzaman, J. A. Zapien, and A. Ruotolo, "Enhanced electrochemical performance of ZnO nanorod core/polypyrrole shell arrays by graphene oxide," *Electrochimica Acta*, vol. 187, pp. 517–524, 2016.

[34] N. Ghaemi and P. Daraei, "Enhancement in copper ion removal by PPy@Al_2O_3 polymeric nanocomposite membrane," *Journal of Industrial and Engineering Chemistry*, vol. 40, pp. 26–33, 2016.

[35] J. Zhang, Y. Liu, H. Guan, Y. Zhao, and B. Zhang, "Decoration of nickel hydroxide nanoparticles onto polypyrrole nanotubes with enhanced electrochemical performance for supercapacitors," *Journal of Alloys and Compounds*, vol. 721, pp. 731–740, 2017.

[36] Y. Liu, H. Wang, J. Zhou et al., "Graphene/polypyrrole intercalating nanocomposites as supercapacitors electrode," *Electrochimica Acta*, vol. 112, pp. 44–52, 2013.

[37] J. Światowska-Mrowiecka, S. Zanna, K. Ogle, and P. Marcus, "Adsorption of 1, 2-diaminoethane on ZnO thin films from p-xylene," *Applied Surface Science*, vol. 254, no. 17, pp. 5530–5539, 2008.

[38] G. Ramos-Sánchez, M. M. Bruno, Y. R. J. Thomas, H. R. Corti, and O. Solorza-Feria, "Mesoporous carbon supported nanoparticulated $PdNi_2$: a methanol tolerant oxygen reduction electrocatalyst," *International Journal of Hydrogen Energy*, vol. 37, no. 1, pp. 31–40, 2012.

[39] D. Bresser, E. Paillard, R. Kloepsch et al., "Carbon coated $ZnFe_2O_4$, nanoparticles for advanced lithium-ion anodes," *Advanced Energy Materials*, vol. 3, no. 4, pp. 513–523, 2013.

[40] J. Wu, C. Chen, Y. Hao, and C. Wang, "Enhanced electrochemical performance of nanosheet ZnO/reduced graphene oxide composites as anode for lithium-ion batteries," *Colloids and Surfaces A: Physicochemical and Engineering Aspects*, vol. 468, pp. 17–21, 2015.

[41] M. H. Jung, "Carbon-coated ZnO mat passivation by atomic-layer-deposited HfO_2 as an anode material for lithium-ion batteries," *Journal of Colloid and Interface Science*, vol. 505, pp. 631–641, 2017.

[42] B. Joshi, E. Samuel, Y. I. Kim et al., "Hierarchically designed ZIF-8-derived Ni@ZnO/carbon nanofiber freestanding composite for stable Li storage," *Chemical Engineering Journal*, vol. 351, pp. 127–134, 2018.

[43] G. Karunakaran, M. Kundu, S. Kumari et al., "ZnO/Cu_2MgO_3 hollow porous nanocage: a new class of hybrid anode material for advanced lithium-ion batteries," *Journal of Alloys and Compounds*, vol. 763, pp. 94–101, 2018.

[44] Q. Xie, L. Lin, Y. Ma et al., "Synthesis of ZnO-Cu-C yolk-shell hybrid microspheres with enhanced electrochemical properties for lithium ion battery anodes," *Electrochimica Acta*, vol. 226, pp. 79–88, 2016.

[45] T. Kim, H. Kim, J. M. Han, and J. Kim, "ZnO-embedded N-doped porous carbon nanocomposite as a superior anode material for lithium-ion batteries," *Electrochimica Acta*, vol. 253, pp. 190–199, 2017.